An In Situ Gelled Polymer Electrolyte to Stabilize Lithium–Air Batteries

Zi-Wei Li, Yu-Long Liang, Jin Wang, Jun-Min Yan, Jian-Wei Liu, Gang Huang, Tong Liu,* and Xin-Bo Zhang*

Gel polymer-based lithium batteries exhibit a unique combination of advantageous properties, including the favorable interfacial contact characteristic of liquid-state batteries and the inherent stability of solid-state batteries. For Li–air batteries operated in the semi-open atmosphere, implementing in situ synthesized gel polymer electrolytes (GPEs) is effective in mitigating the environment-induced challenges. In this study, a dimethyl sulfoxide (DMSO)-based GPE in situ initiated by the toluene-2,4-diisocyanate (TDI) and 1,4-benzenediboronic acid (BDBA) is designed to enable the stable operation of lithium–air batteries. The integration of in situ polymerization and polyvinyl alcohol's functional group engineering not only brings benefits to the interfacial contact and electrochemical stability of the battery but also mitigates the moisture sensitivity and volatility of the DMSO electrolyte in the ambient environment. In addition, the GPE can promote the formation of a robust protection film on the lithium surface. As a result, the designed GPE makes the batteries fully leverage their outstanding cycling stability in the ambient environment (241 cycles at 500 mA g^{-1} and 1000 mAh g^{-1}). Moreover, an optimized Li–air pouch cell structure incorporating the GPE achieves a boasted energy density of 757.5 Wh kg^{-1}, providing a significant technical pathway to bring Li–O$_2$ batteries to practical Li–air batteries.

1. Introduction

Lithium–oxygen (Li–O$_2$) batteries have garnered substantial attention as promising contenders among the diverse energy storage systems due to their exceptionally elevated theoretical energy density of ≈3500 Wh kg^{-1}, which is an order of magnitude higher than the advanced lithium-ion batteries (≈350 Wh kg^{-1}).[1–3] Despite the notable theoretical energy density, the practical implementation of Li–O$_2$ batteries often encounters limitations in achieving optimal performance when operated in the real ambient environment. This performance divergence can be ascribed to the exigent challenges induced by the semi-open nature of lithium–air (Li–air) batteries, such as the evaporation and degradation of the liquid organic electrolytes and the parasitic reactions of the lithium anode with carbon dioxide and water.[4] These intricate problems hinder the transition of Li–O$_2$ batteries into authentic Li–air batteries.

To this end, a range of optimization strategies centering on conquering the challenges of Li–air batteries has been proposed. These strategies encompass the introduction of oxygen-selective membranes, the engineering of protective layers on the lithium anode surface, and the optimization of electrolyte composition.[5–7] Among them, the utilization of gel polymer electrolytes (GPEs) emerges as a particularly promising avenue.[8,9] The GPEs with liquid electrolytes (LEs) encapsulated in the polymer network could integrate the high ionic conductivity of LEs and the high stability of solid electrolytes together.[7] At the same time, the crosslinked polymer chains in the GPEs could effectively limit the movement of the LEs and consequently inhibit their evaporation and leakage.[4] Furthermore, the compositional design of GPEs may also contribute positively to stabilizing the lithium anode by facilitating the formation of robust solid electrolyte interphase (SEI) films.[10,11] Importantly, the above benefits from GPEs make the obviation of supplementary protective structural design of batteries operated in the ambient air become possible.[12]

Despite promising, achieving the optimal balance between the required Li–air battery performance traits of large capacity, high-rate capability, and system stability poses notable challenges for conventional GPEs. An important limiting factor is that the general GPEs are difficult to fully couple with the mature liquid solvents of Li–O$_2$ batteries, like dimethyl sulfoxide (DMSO), which possesses advantageous characteristics, including high oxygen solubility, good oxygen reduction reaction/oxygen evolution

Z.-W. Li, Y.-L. Liang, J.-M. Yan
Key Laboratory of Automobile Materials
Ministry of Education, Department of Materials Science and Engineering
Jilin University
Changchun 130022, China
Z.-W. Li, Y.-L. Liang, J. Wang, J.-W. Liu, G. Huang, T. Liu, X.-B. Zhang
State Key Laboratory of Rare Earth Resource Utilization
Changchun Institute of Applied Chemistry
Chinese Academy of Sciences
Changchun 130022, China
E-mail: tongliu@ciac.ac.cn; xbzhang@ciac.ac.cn
J.-W. Liu, G. Huang, T. Liu, X.-B. Zhang
University of Science and Technology of China
Hefei 230026, China
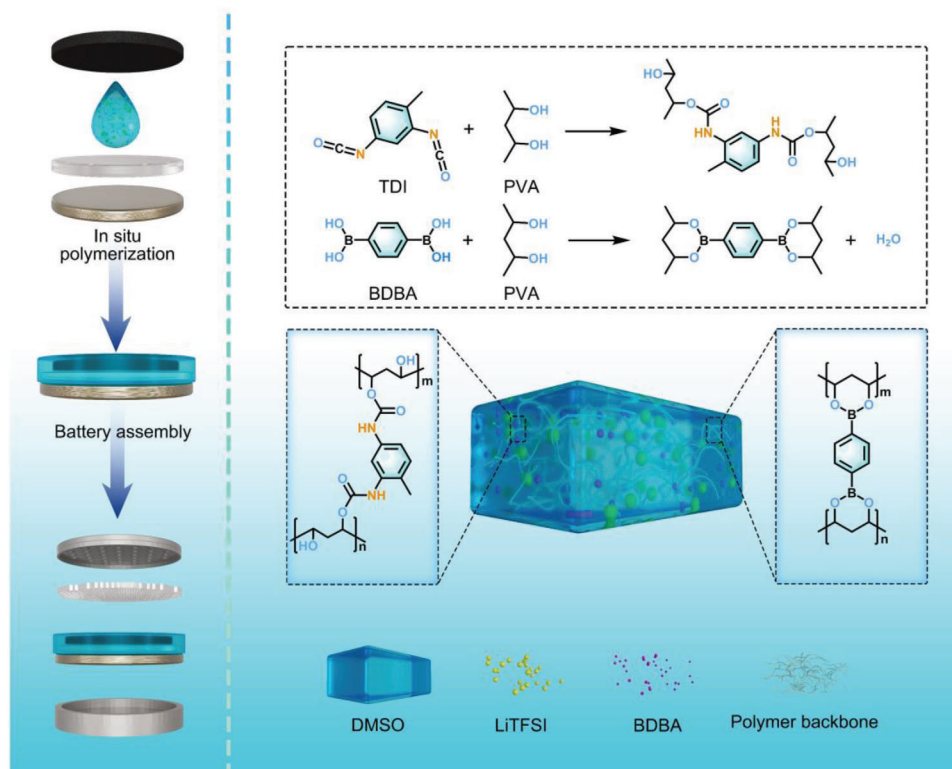
Scheme 1. Schematic illustration of the synthesis of the PTB electrolyte.

reaction (ORR/OER) response, and a high donor number (DN).[13] However, the easily volatile nature, sensitivity to water, and poor stability against the lithium anode of DMSO limit its application in the semi-open Li–air battery system.[14,15] These limitations put forward rigorous requirements for constructing suitable DMSO-based GPEs to realize the stable operation of Li–air batteries. Up to now, the utilization of DMSO-based electrolytes in the authentic atmospheric environment typically necessitates the incorporation of specialized gas filtration membranes or complex artificial interface layers.[16,17] The introduction of these additional components would inevitably curtail the overall energy density of batteries and also complicate the battery manufacturing process.

Herein, a multifunctional GPE (polyvinyl alcohol/toluene-2,4-diisocyanate/1,4-benzenediboronic acid, PVA-TDI-BDBA, termed as PTB) with high compatibility to the DMSO has been thoughtfully devised to address the paradoxical challenges of the DMSO-based electrolytes. The introduction of the TDI and BDBA could realize the in situ polymerization of the electrolyte through their reaction with the —OH groups in PVA, concurrently guaranteeing intimate interfacial contact and strengthening the thermal stability and hydrophobicity of the GPE.[18] Meanwhile, the inclusion of a certain amount of BDBA could engender boronate centers to facilitate the adsorption of Li salt anions and consequently augment the transfer number of Li+ ions.[19–21] Moreover, the GPE could also contribute to constructing robust SEI films rich in B-O species and LiF to improve the compatibility of DMSO to the lithium anode and protect the lithium anode from air-induced corrosion.[22]

As a result, the elaborately formulated PTB makes the Li–air batteries achieve significantly improved cycling stability of 241 cycles at 500 mA g^{-1} and 1000 mAh g^{-1}, notably surpassing the performance of liquid DMSO-based battery with a lifetime of only 54 cycles. More importantly, the energy density quandary of the real Li–air batteries could be conquered by leveraging the PTB in conjunction with the comprehensive battery structure optimizations. The PTB-based Li–air pouch cell demonstrates a remarkable energy density of 757.5 Wh kg^{-1} in the ambient atmosphere, approximately five times to that of the liquid DMSO-based battery (149.6 Wh kg^{-1}).

2. Results and Discussion

As illustrated in **Scheme 1**, PVA was selected as the polymer network for the GPE due to its long-chain rendered high structural stability.[23] However, PVA alone cannot construct appropriate GPE for Li–air batteries due to its abundant —OH groups, generally resulting in water contamination to the lithium anode. Since the —OH groups in PVA can be readily replaced by other polar groups while retaining a stable long-chain structure,[24] it could serve as an excellent GPE starting point for modification. In this consideration, TDI and BDBA were selected to initiate the in situ polymerization of the DMSO-PVA electrolyte. The TDI could react with the —OH groups in PVA to form carbamate groups, enhancing the hydrophobicity of the GPE.[18] For further introducing BDBA, on the one hand, it enables the full consumption of the residual —OH groups in the PVA; on the other hand, it facilitates the adsorption of Li salt anions and construction of
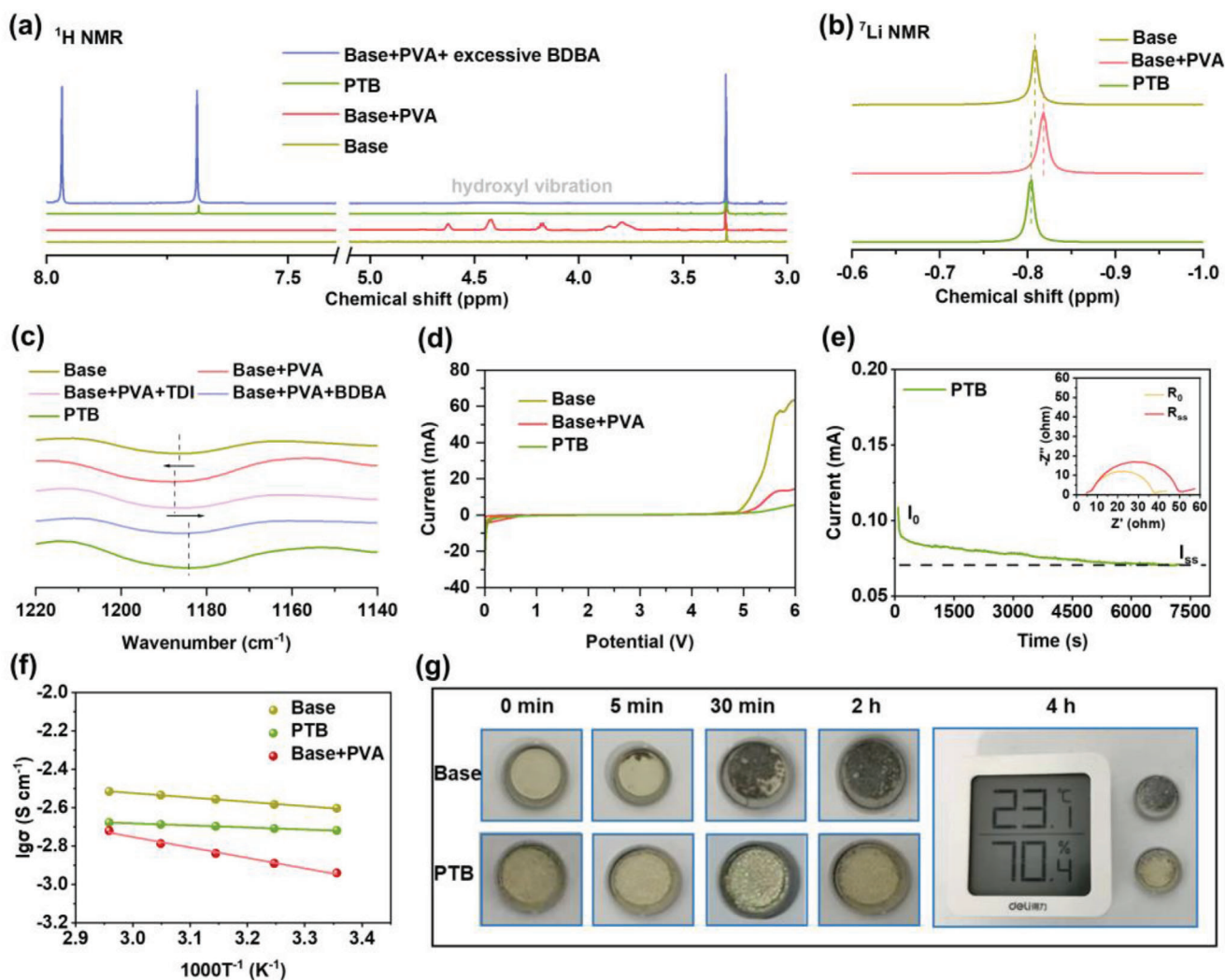
**ADVANCED
SCIENCE NEWS**

www.advancedsciencenews.com

**ADVANCED
ENERGY
MATERIALS**

www.advenergymat.de

Figure 1. a) ^1H NMR spectra of the electrolytes with different component ratios. b) Comparison of the ^7Li NMR shift between different electrolytes. c) Infrared spectra and d) linear sweep voltammetry curves of different electrolytes. e) Chronoamperometric curve of the Li/Li symmetric cell with the PTB. Inset is the corresponding EIS curves before and after potentiostatic DC polarization. f) Temperature-dependent ionic conductivity plots of different electrolytes. g) Air stability test of the lithium metal with the protection of base or PTB electrolyte.

boron-rich SEI film on the Li anode surface. The combination of TDI and BDBA could solve the shortcomings of the PVA added base electrolyte (1 M LiTFSI/DMSO) and, accordingly, makes the obtained GPE cater to the needs of stable operation of Li–air batteries.

The detailed synthesis process of PTB was quantitatively analyzed by Nuclear Magnetic Resonance (NMR) (**Figure 1a**). In the base electrolyte containing PVA, multiple hydroxyl vibration peaks can be clearly observed.[25] However, these peaks vanish after the introduction of TDI and BDBA, indicating the sufficient polymerization induced by the complete consumption of the —OH groups in the PVA. The existence of a moderate BDBA in the PTB displays a characteristic peak corresponding to the ortho-H of phenylenediborate. With further increasing the BDBA content, an abundance of free BDBA and anhydride appears, along with the emergence of distinct peaks related to the ortho and meta hydrogens of the benzene ring. Introducing an overdose of BDBA results in a noticeable rise in free BDBA molecules

and consequently generates excessive water from the unstable BDBA. Therefore, it is necessary to regulate the concentration of BDBA to prevent any side reactions with the lithium anode.[20] Fourier transform infrared spectroscopy (FTIR) characterization was then performed to provide detailed information on the functional group changes at each reaction stage of the PTB (Figure S1, Supporting Information). For PTB, the significant reduction of the -OH peak intensity at 3300–3400 cm^{-1} and the absence of the N=C=O peak at 2270 cm^{-1} indicate the reaction of the isocyanate groups in TDI with the —OH groups in PVA.[26] The appearance of peaks at 1718 cm^{-1} (stretching vibrations of C—O and C=O), 1601 cm^{-1} (stretching vibration of benzene ring), and 1540 cm^{-1} (bending vibration of secondary aromatic amine) confirms the incorporation of TDI into the PVA chain and formation of carbamate groups.[27] Additionally, characteristic peaks at 1294 cm^{-1} (B—O stretching) and 665 cm^{-1} (boronate bond) also appear, revealing that the BDBA involves in the polymerization process to further consume the residual —OH groups in PVA.[21]

ADVANCED
SCIENCE NEWS

www.advancedsciencenews.com

ADVANCED
ENERGY
MATERIALS

www.advenergymat.de

Combining the NMR and FTIR results, it is clear that the PTB inherits the boronic esters from BDBA and carbamate groups from TDI, inducing the in situ polymerization of PVA added base electrolyte by the sufficient consumption of the -OH groups in PVA.

After this, X-ray diffraction (XRD) measurement was conducted to check the crystallinity of the PTB. As shown in Figure S2 (Supporting Information), the peaks corresponding to the lithium salt cannot be detected in the PTB, signifying the complete dissolution of the lithium salt and thus enriching the freely moving Li$^+$ ions.[28] This can be partly attributed to that the boronate linkages in the gel network could act as typical Lewis acid sites to attract the TFSI$^-$ anion to facilitate the release of Li$^+$ ions from the lithium salts.[21] The weakening of the binding strength between the TFSI$^-$ and Li$^+$ ions is reflected in the downshift of the ^{7}Li NMR peak for the PTB when compared to the base electrolyte (Figure 1b).[29–31] The interaction of anions with the polymer linkages in the PTB mitigates the influence of electron cloud density on Li$^+$ ions, resulting in a downfield shift of the ^{7}Li peak, while the hydroxyl groups in the original PVA chains renders the upshift of the ^{7}Li peak.[32,33] In the FTIR spectra (Figure 1c), apparent changes in the —CF$_3$ stretching peaks from the TFSI$^-$ can be observed after introducing different components to the base electrolyte. The effect of —OH groups in PVA brings a blue shift of the —CF$_3$ peak, while the TDI-caused —OH content decrease enables the back shift of the peak. After adding BDBA, it could further strengthen the ability of the polymer chain to attract the TFSI$^-$ anions to make the redshift of —CF$_3$ peak.[30]

Then, the intrinsic properties of the designed electrolytes were investigated. As indicated in Figure 1d, the addition of PVA polymer into the base electrolyte could improve the electrochemical oxidation stability,[34] and the antioxidant stability further increases to 5.2 V for the PTB due to the sufficient polymerization rendered efficient trap of DMSO. Besides the improved oxidation stability, the PTB also exhibits a higher Li$^+$ ion transfer number than the base electrolyte (0.54 vs 0.46, Figure 1e; Figure S3, Supporting Information), which can be attributed to the anionic adsorption ability of the boronate groups. However, the inhibition of Li$^+$ migration by the rich hydroxyl groups of PVA makes the PVA-added electrolyte only exhibit a Li$^+$ ion transfer number of 0.38, highlighting the effectiveness of the introduced TDI and BDBA (Figure S4, Supporting Information). The temperature-dependent ionic conductivity plots of the PTB and base electrolyte with/without PVA were subsequently studied to check their Arrhenius activation energies. It can be seen from Figure 1f that the activation energy of the PTB is less than half of the base electrolyte (1.99 vs 4.33 kJ mol^{-1}), suggesting a significant improvement in the Li$^+$ migration kinetic.[35] For the base electrolyte with PVA, the activation energy experiences a significant increase (10.43 kJ mol^{-1}).

Considering the semi-open nature of the Li–air batteries, the volatility of the electrolyte is one of the key factors that determine the battery performance. Different from the evident weight loss of the base electrolyte above 80 °C, the 3D polymer network structure of the PTB could effectively lock the DMSO with limited electrolyte volatilization until 100 °C (Figure S5, Supporting Information), meeting the volatility and thermal stability requirements of Li–air battery operating conditions.[36] For the anode side, the hydrophobicity of the electrolyte is of vital importance to block the water attack induced Li corrosion. Figure S6 (Sup-

porting Information) gives the contact angle measurement of the electrolytes with water. It is clear that the base electrolyte could rapidly absorb the water, and the electrolyte polymerized solely with BDBA also exhibits poor hydrophobicity with a contact angle of only 44.7°. For PTB, significantly improved hydrophobicity is realized. This high hydrophobicity can be further supported by the valid inhibition of water diffusion caused lithium metal erosion in the high humidity environment of 70%RH, while the lithium metal with the base electrolyte displays severe corrosion (Figure 1g). In addition, significant degradation is observed for the lithium metal with the PVA-added electrolyte in the 33% RH environment, even faster than the base one (Figure S7, Supporting Information). This can be ascribed to that the large number of hydrophilic —OH groups in the PVA causes rapid water intrusion to corrode the lithium metal. Therefore, the base electrolyte containing only PVA with limited Li$^+$ transfer kinetic and poor compatibility to the lithium anode is not suitable for Li–air batteries. On the contrary, the designed PTB possesses the basic properties (high oxidation stability, improved Li$^+$ diffusion kinetic, low volatility, etc.) that meet the stringent requirements of high-performance running of Li–air batteries.

Li/Li symmetric batteries were then assembled to further investigate the compatibility between the PTB and lithium anode. As shown in **Figure 2a**, the PTB-based battery could operate stably for over 300 h, six times longer than the battery with the base electrolyte. Moreover, different from the flat surface of the lithium anode cycled in the PTB, the one in the base electrolyte experiences serious damage with obvious surface pulverization (Figure 2b,c), suggesting that the designed PTB possesses the ability to protect the lithium anode from dendrite growth and corrosion reactions. Despite the introduction of BDBA could result in water generation according to the reaction in Scheme 1, it would not influence the anode protection function of the PTB if the BDBA's amount is controlled appropriately (Figure S8, Supporting Information).[20] Additionally, even cycled in the Li–air batteries, the lithium anode in the PTB-based battery still exhibits a relatively flat surface with fewer parasitic reactions than the anode in the battery with the base electrolyte (Figure 2d,e). The composition evolution of the lithium anode surfaces was also investigated by X-ray photoelectron spectroscopy (XPS) measurement. The O 1s and B 1s spectra show the presence of B—O bond peaks on the lithium anode surface cycled in the PTB-based battery (Figure 2f,g), while these peaks cannot be observed on the anode in the base electrolyte, signifying that the PTB could facilitate the construction of a SEI film containing B—O species on the lithium surface.[20] Meanwhile, since the LiF is a beneficial SEI component to protect the lithium anode, the higher intensity of the LiF peak in the F 1s spectra of the lithium anode in the PTB further strengthens the anode protection ability of the PTB-derived SEI film (Figure 2h).[20,37] For the anode in the base electrolyte, the main components of the SEI film are LiOH and Li$_2$CO$_3$ (Figure 2f,i), which is primarily attributed to the by-products formed from the reaction of lithium and dissolved CO$_2$ and H$_2$O in the electrolyte.[38] The presence of B—O species, increased amount of LiF, and reduced amounts of LiOH and Li$_2$CO$_3$ on the lithium metal surface in the PTB demonstrate the effectiveness of the PTB in constructing powerful SEI films to protect the lithium anode, improving the compatibility between the PTB and lithium anode. Also, the above results certify that the challenges faced by the base electrolyte in
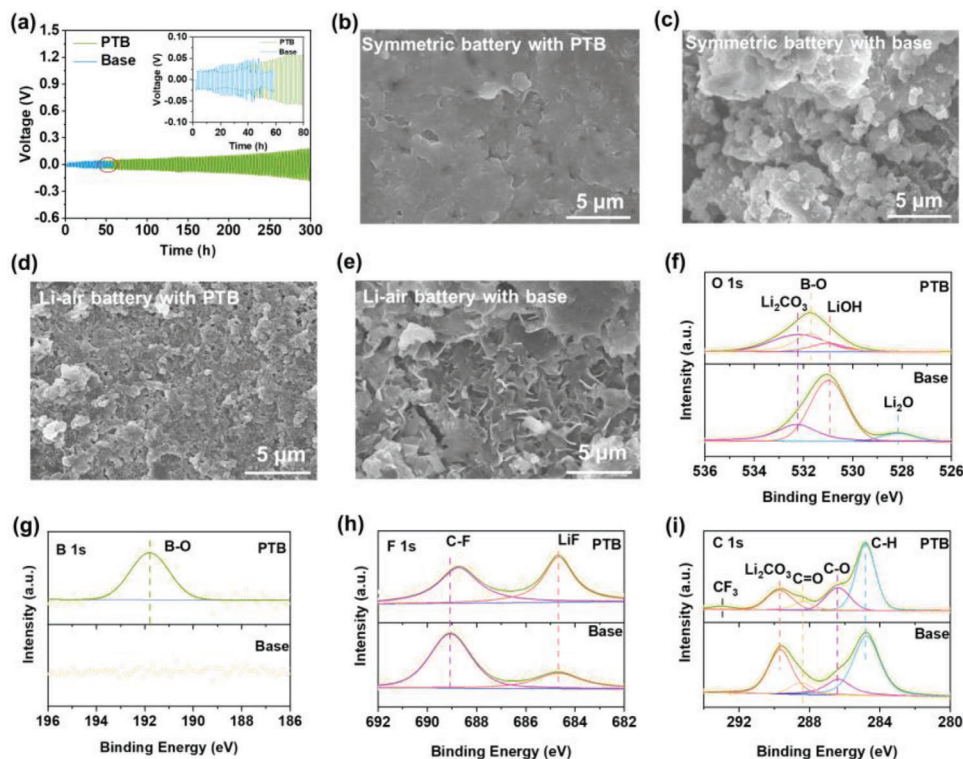
**ADVANCED
SCIENCE NEWS**

www.advancedsciencenews.com

**ADVANCED
ENERGY
MATERIALS**

www.advenergymat.de

Figure 2. a) Cycling performance of Li/Li symmetric batteries with the base or PTB electrolyte at a current density of 0.3 mA cm^{-2}. SEM images of the lithium surface morphology after 20 cycles in symmetric batteries with the b) PTB and c) base electrolyte. SEM images of the surface morphology of lithium anodes after 20 cycles in Li–air batteries with the d) PTB and e) base electrolyte. XPS spectra of f) O 1s, g) B 1s, h) F 1s, and i) C 1s for the Li anodes after 20 cycles in Li–air batteries.

the ambient environment have been successfully conquered by the designed PTB, providing the promise of constructing high-performance Li–air batteries.

To verify the practicability of the PTB in Li–air batteries, coin-type batteries with different electrolytes working in the ambient environment were first assembled. For the PTB-based battery, the scanning electron microscopy (SEM) image shows that the in situ formed PTB well covers the cathode surface, ensuring sufficient and close interfacial contact (Figure S9a, Supporting Information). The cyclic voltammetry (CV) curve of the PTB-based battery confirms that the battery basically follows the typical oxygen electrochemical reactions (Figure S9b, Supporting Information), and the SEM image of the discharged cathode shows obvious particle-type discharge products (Figure S9c, Supporting Information).[39] XRD measurement reveals that the discharge products in the PTB-based battery consist of a mixture of Li_2O_2 and LiOH (Figure S9d, Supporting Information), which is a comprehensive effect of the air component, cathode, and electrolyte.[16] The mixed products can be sufficiently decomposed after the subsequent charge process, indicating the high reversibility of the discharge products. **Figure 3a** illustrates that the PTB-based battery with Super P (SP) cathode could deliver a significantly larger full discharge capacity than the battery with the base electrolyte at 1000 mA g^{-1} (5362 vs 3504 mAh g^{-1}). For the cycling performance, the differences in thermal stability and compatibility with the lithium anode between the PTB and base electrolyte results in a big discrepancy in the battery lifetime when cycled

with a limited capacity of 2000 mAh g^{-1} at 1000 mA g^{-1} and 60 °C (Figure 3b). The high working temperature induced rapid evaporation of the DMSO and exacerbated parasitic reactions of the lithium anodes, leading to an increase in the initial polarization of the battery with the base electrolyte.[15,40] In contrast, the PTB could alleviate the issues encountered by the base electrolyte, making the PTB-based battery exhibit low initial polarizations and prolonged cycle life. This can be further clearly observed by the representative charge–discharge curves of the Li–air batteries with SP cathodes and different electrolytes (Figure 3c,d). The battery with the base electrolyte displays constant large polarizations and quickly fails just after 34 cycles, while the PTB-based battery runs stably for 143 cycles at 1000 mAh g^{-1} and 500 mA g^{-1}. Additionally, when the PTB is paired with the Ru/SP cathode to assemble Li–air batteries, the cycling lifetime can be further boosted to 241 cycles, nearly five times to the battery with the base electrolyte (Figure 3e; Figure S10, Supporting Information). Figure S11 (Supporting Information) gives the impedance evolution of Li–air batteries with different electrolytes. The batteries with the electrolyte containing PVA were excluded due to the high impedance caused by the violent reaction between the abundant hydroxyl groups in PVA and lithium metal. Unlike the rapid interfacial impedance increase of the battery with the base electrolyte as cycling goes on, the PTB-based battery exhibits relatively stable interfacial impedance with a slow growth trend, proving the high efficacy of the PTB in stabilizing the electrolyte-electrode interface. In sum, the designed PTB with
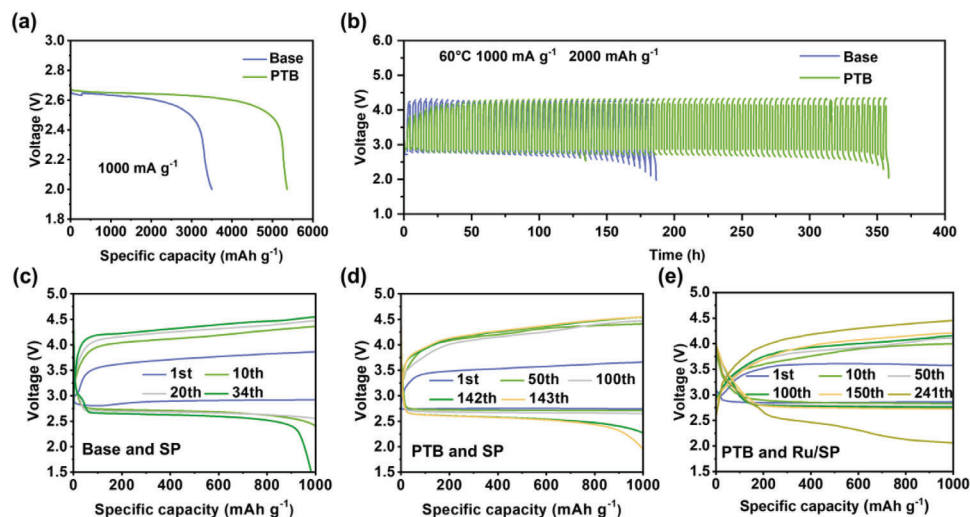
Figure 3. a) Full discharge performance of the Li–air batteries with SP cathodes and different electrolytes at 1000 mA g^{-1} and room temperature. b) Cycling performance of the Li–air batteries with SP cathodes and different electrolytes with a limited capacity of 2000 mAh g^{-1} at 1000 mA g^{-1} and 60 °C. Charge–discharge curves of the SP cathode-based Li–air batteries with the c) base electrolyte and d) PTB. e) Charge–discharge curves of the Li–air batteries with the Ru/SP cathode and PTB electrolyte.

the advantages of facilitating mass transfer, maintaining interface stability, and resisting environmental interference is well suitable for the Li–air batteries operated in the ambient environment and makes the battery deliver outstanding electrochemical performance.

Besides coin-type batteries, amplified Li–air pouch cells were also constructed to demonstrate the beneficial effects of the PTB brought to the cell performance (**Figure 4a**). It can be seen from Figure 4c that the PTB-based cell exhibits a discharge capacity of more than four times that of the cell with the base elec-
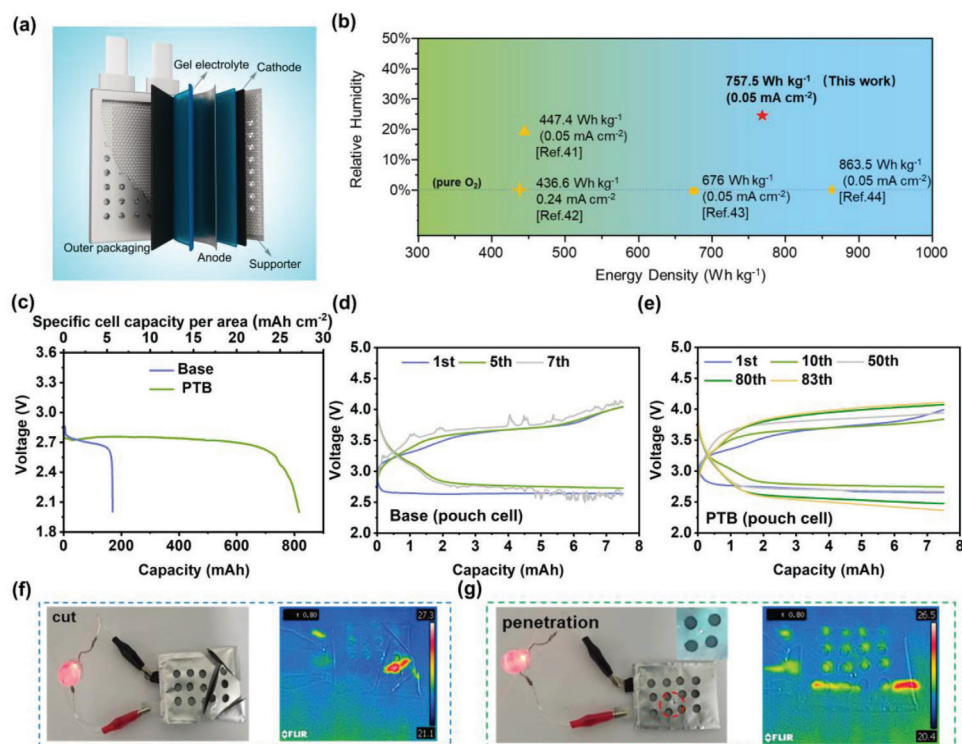

Figure 4. a) Schematic illustration of a Li–air pouch cell. b) Comparison of the energy densities of Li–O$_2$/Li–air batteries reported in recent years. c) Full discharge capacities of the Li–air pouch cells with different electrolytes. Cycling performance of the Li–air pouch cells with the Ru/SP cathodes using d) base electrolyte and e) PTB at 0.2 mA cm^{-2} and 0.5 mAh cm^{-2}. Safety tests of the PTB-based Li–air pouch cells: Optical and infrared photos after f) cut and g) acupuncture.

trolyte. When calculated based on the core body of the cell (anode, cathode, separator, and electrolyte, Figures S12 and S13, and Tables S1 and S2, Supporting Information), the energy density of the optimized PTB-based cell could reach a high value of 757.5 Wh kg^{-1}, whereas the cell with the base electrolyte only delivers 149.6 Wh kg^{-1}, highlighting the advantage of the PTB in promoting the cell energy density. It should be mentioned that the energy density of the PTB-based cell achieved here is superior to most of the recently reported Li–O$_2$/Li–air cells (Figure 4b).[41–44] Then, the cycling stability of Li–air pouch cells was checked to evaluate their actual application potential in long-term servicing. The cell with the base electrolyte displays a violent jitter in the discharge curve just after seven cycles (Figure 4d).[45–47] For the PTB-based cell, it can normally run for 83 cycles (Figure 4e), indicating that the long-term stability of the coin-type PTB-based batteries can be well inherited to the large-sized pouch cells. Importantly, the performance achieved here has strong competitiveness when compared with other reports (Table S3, Supporting Information). The power density of Li–air pouch cells has also been investigated (Figure S14, Supporting Information), and the issue of mass transfer hindrance at high current densities needs to be further addressed.[48] Figure 4f,g gives the safety test results of the PTB-based pouch cells. Even after corner cutting and puncture, the battery can still work well to power the bulb without any observable sign of short circuit. Meanwhile, the infrared temperature measurement shows that the local temperatures of the damaged areas just experienced a slight increase, demonstrating the high cell safety rendered by the PTB. The above results clearly certify that the designed PTB has strong practicability in improving the performance of large-sized Li–air cells.

3. Conclusion

In conclusion, a new kind of gel polymer electrolyte that could cater to the rigorous requirements of high-performance running of Li–air batteries in the ambient environment has been elaborately designed by employing the PVA's functional group engineering and in situ polymerization together. The designed PTB can not only address the issues of moisture sensitivity, volatility, and poor anode compatibility associated with the DMSO-based electrolyte, but also bring benefits to the Li$^+$ ion transfer kinetic and lithium anode protection. As a result, the PTB-based Li–air batteries could stably operate for 241 cycles at 1000 mAh g^{-1} and 500 mA g^{-1} in the ambient environment, and the Li–air pouch cell could deliver an energy density as high as 757.5 Wh kg^{-1}. The results presented here provide a promising pathway to bring Li–air batteries one-step closer to becoming a practical technology.

Supporting Information

Supporting Information is available from the Wiley Online Library or from the author.

Conflict of Interest

The authors declare no conflict of interest.

Data Availability Statement

The data that support the findings of this study are available from the corresponding author upon reasonable request.

[1] L. Ma, T. Yu, E. Tzoganakis, K. Amine, T. Wu, Z. Chen, J. Lu, *Adv. Energy Mater.* **2018**, *8*, 1800348.
[2] G. Zheng, T. Yan, Y. Hong, X. Zhang, J. Wu, Z. Liang, Z. Cui, L. Du, H. Song, *Nat. Commun.* **2023**, *14*, 2268.
[3] X. Huang, X. Zhao, Z. Wang, L. Wang, X. Zhang, *J. Mater. Chem.* **2012**, *22*, 3764.
[4] T. Liu, J. Zhang, W. Han, J. Zhang, G. Ding, S. Dong, G. Cui, *J. Electrochem. Soc.* **2020**, *167*, 070527.
[5] J. Zhang, W. Xu, X. Li, W. Liu, *J. Electrochem. Soc.* **2010**, *157*, A940.
[6] Z. Guo, J. Li, Y. Xia, C. Chen, F. Wang, A. G. Tamirat, Y. Wang, Y. Xia, L. Wang, S. Feng, *J. Mater. Chem. A* **2018**, *6*, 6022.
[7] Y. G. Cho, C. Hwang, D. S. Cheong, Y. S. Kim, H. K. Song, *Adv. Mater.* **2019**, *31*, 1804909.
[8] T. Liu, Z. Chang, Y. Yin, K. Chen, Y. Zhang, X. Zhang, *Solid State Ionics* **2018**, *318*, 88.
[9] J. Gou, Z. Zhang, S. Wang, J. Huang, K. Cui, H. Wang, *Adv. Mater.* **2023**, 2309677.
[10] D. Chen, M. Zhu, P. Kang, T. Zhu, H. Yuan, J. Lan, X. Yang, G. Sui, *Adv. Sci.* **2022**, *9*, 2103663.
[11] K. Mu, D. Wang, D. Dong, Q. Liu, Z. Song, W. Xu, P. Yao, Y. Chen, B. Yang, C. Li, L. Tian, C. Zhu, J. Xu, *Adv. Mater.* **2023**, *35*, 2304686.
[12] X. Lei, X. Liu, W. Ma, Z. Cao, Y. Wang, Y. Ding, *Angew. Chem., Int. Ed.* **2018**, *57*, 16131.
[13] L. Johnson, C. Li, Z. Liu, Y. Chen, S. A. Freunberger, P. C. Ashok, B. B. Praveen, K. Dholakia, J. M. Tarascon, P. G. Bruce, *Nat. Chem.* **2014**, *6*, 1091.
[14] N. Feng, P. He, H. Zhou, *Adv. Energy Mater.* **2016**, *6*, 1502303.
[15] M. J. Trahan, S. Mukerjee, E. J. Plichta, M. A. Hendrickson, K. M. Abraham, *J. Electrochem. Soc.* **2012**, *160*, A259.
[16] J. Lei, Z. Gao, L. Tang, L. Zhong, J. Li, Y. Zhang, T. Liu, *Adv. Sci.* **2022**, *9*, 2103760.
[17] A. Jaradat, C. Zhang, S. K. Singh, J. Ahmed, A. Ahmadiparidari, L. Majidi, S. Rastegar, Z. Hemmat, S. Wang, A. T. Ngo, L. A. Curtiss, M. Daly, A. Subramanian, A. Salehi-khojin, *Small* **2021**, *17*, 2102072.
[18] F. Jiang, Y. L. Hsieh, *ACS Appl. Mater. Interfaces* **2017**, *9*, 2825.
[19] Y. Han, Y. Zhou, J. Zhu, Z. Sun, L. Xu, C. Li, Y. Ma, H. Zhang, Y. Chen, *Sci. China Mater.* **2020**, *63*, 2344.

**ADVANCED
SCIENCE NEWS**

www.advancedsciencenews.com

**ADVANCED
ENERGY
MATERIALS**

www.advenergymat.de

[20] Z. Huang, J. Ren, W. Zhang, M. Xie, Y. Li, D. Sun, Y. Shen, Y. Huang, *Adv. Mater.* **2018**, *30*, 1803270.

[21] G. M. Peters, X. Chi, C. Brockman, J. L. Sessler, *Chem. Commun.* **2018**, *54*, 5407.

[22] X. B. Cheng, S. J. Yang, Z. Liu, J. X. Guo, F. N. Jiang, F. Jiang, X. Xiong, W. B. Tang, H. Yuan, J. Q. Huang, Y. Wu, Q. Zhang, *Adv. Mater.* **2024**, *36*, 2307370.

[23] S. Hao, Z. Ma, Y. Zhao, L. Kong, H. He, G. Shao, X. Qin, W. Gao, *ACS Omega* **2020**, *5*, 8299.

[24] Y. Saito, M. Okano, K. Kubota, T. Sakai, J. Fujioka, T. Kawakami, *J. Phys. Chem. B* **2012**, *116*, 10089.

[25] C. Li, M. She, X. She, J. Dai, L. Kong, *J. Appl. Polym. Sci.* **2014**, *131*, 39872.

[26] A. Strakšys, T. Kochane, S. Budriene, *Chemija* **2013**, *24*, 160.

[27] Q. Hu, G. Huang, J. Zheng, H. Su, C. Guo, *J. Polym. Res.* **2012**, *19*, 1.

[28] W. Fan, N. W. Li, X. Zhang, S. Zhao, R. Cao, Y. Yin, Y. Xing, J. Wang, Y. G. Guo, C. Li, *Adv. Sci.* **2018**, *5*, 1800559.

[29] C. M. Burke, V. Pande, A. Khetan, V. Viswanathan, B. D. McCloskey, *Proc. Natl. Acad. Sci. USA* **2015**, *112*, 9293.

[30] J. Xiang, Y. Zhang, B. Zhang, L. Yuan, X. Liu, Z. Cheng, Y. Yang, X. Zhang, Z. Li, Y. Shen, J. Jiang, Y. Huang, *Energy Environ. Sci.* **2021**, *14*, 3510.

[31] J. Adebahr, M. Forsyth, D. R. Macfarlane, P. Gavelin, P. Jacobsson, *Solid State Ionics* **2002**, *147*, 303.

[32] M. C. Masiker, C. L. Mayne, B. J. Boone, A. M. Orendt, E. M. Eyring, *Magn. Reson. Chem.* **2010**, *48*, 94.

[33] M. R. Lukatskaya, J. I. Feldblyum, D. G. Mackanic, F. Lissel, D. L. Michels, Y. Cui, Z. Bao, *Energy Environ. Sci.* **2018**, *11*, 2876.

[34] Y. D. Kim, Y. K. Jo, N. J. Jo, *J. Nanosci. Nanotechno.* **2012**, *12*, 3529.

[35] Y. Yu, G. Huang, J.-Y. Du, J.-Z. Wang, Y. Wang, Z.-J. Wu, X.-B. Zhang, *Energy Environ. Sci.* **2020**, *13*, 3075.

[36] Y.-H. Zhang, M.-N. Lu, Q. Li, F.-N. Shi, *J. Solid State Chem.* **2022**, *310*, 123072.

[37] C. Xu, B. Sun, T. Gustafsson, K. Edström, D. Brandell, M. Hahlin, *J. Mater. Chem. A* **2014**, *2*, 7256.

[38] C. Zou, X. Zhang, Y. Huang, L. Zhao, W. Ren, Z. Zhao, J. Liu, X. Li, M. Wang, B. Guo, Y. Lin, *Electrochim. Acta* **2022**, *433*, 141245.

[39] H. M. A. Amin, C. Molls, P. P. Bawol, H. Baltruschat, *Electrochim. Acta* **2017**, *245*, 967.

[40] L. P. Hou, X. Q. Zhang, B. Q. Li, Q. Zhang, *Angew. Chem., Int. Ed.* **2020**, *59*, 15109.

[41] J.-G. Zhang, D. Wang, W. Xu, J. Xiao, R. E. Williford, *J. Power Sources* **2010**, *195*, 4332.

[42] H. Lee, D. J. Lee, M. Kim, H. Kim, Y. S. Cho, H. J. Kwon, H. C. Lee, C. R. Park, D. Im, *ACS Appl. Mater. Interfaces* **2020**, *12*, 17385.

[43] S. Matsuda, E. Yasukawa, T. Kameda, S. Kimura, S. Yamaguchi, Y. Kubo, K. Uosaki, *Cell Rep. Phys. Sci.* **2021**, *2*, 100506.

[44] S. Zhao, L. Zhang, G. Zhang, H. Sun, J. Yang, S. Lu, *J. Energy Chem.* **2020**, *45*, 74.

[45] X. Duan, L. Wang, G. Li, X. Liu, M. Wan, J. Du, R. Zhan, W. Wang, Y. Li, S. Tu, Y. Shen, Z. W. Seh, L. Wang, Y. Sun, *Adv. Funct. Mater.* **2022**, *33*, 2210669.

[46] Y. Wu, B. Zhao, X. Zhao, L. Han, Y. Shang, Z. Niu, Y. Liang, X. Zhang, Z. Jiang, F. Li, A. Cao, *Mater. Today* **2022**, *59*, 68.

[47] H.-J. Shin, W.-J. Kwak, D. Aurbach, Y.-K. Sun, *Adv. Funct. Mater.* **2017**, *27*, 1605500.

[48] M. Mehta, V. Bevara, P. Andrei, *J. Power Sources* **2015**, *286*, 299.